METHOD FOR HIGH ACCURACY MEASUREMENTS OF ENERGY COUPLING AND MELTING EFFICIENCY UNDER WELDING CONDITIONS

Paper 1204

Dominik Hipp[1], Achim Mahrle[2], Sebastian Jäckel[1], Eckhard Beyer[1,2], Christoph Leyens[2,3], Uwe Füssel[1]

[1] Institute of Manufacturing Science and Engineering, TU Dresden, PO Box, D-01062 Dresden, Germany
[2] Fraunhofer IWS Dresden, Winterbergstraße 28, D-01277 Dresden, Germany
[3] Institute of Materials Science, TU Dresden, PO Box, D-01062 Dresden, Germany

Abstract

The demands on production processes vastly increased in the last decade. Beside the fulfillment of the fabrication task, a process has to be energy efficient and resource saving to be in line for mass production. For the evaluation of competing technologies or for the optimization of a process regarding these requests the knowledge about the specific process efficiency is crucial. However, the value strongly depends on the chosen process parameters and the environmental conditions, wherefore documented values in literature are inapplicable. Hence, an experimental determination for each individual case is inevitable. Existing methods for the estimation of the process efficiency are either inaccurate or time and cost intensive. Therefore a new method for determining process efficiencies for almost arbitrary materials and process conditions is presented. The method bases on process observation using thermographic imaging and a subsequent adjusted numerical computation of temperature fields. The result of the numerical calculation in combination with the evaluation of the weld seam cross section is the value for the energy coupling efficiency, melting efficiency as well as the overall thermal efficiency. The features of the proposed method are evaluated with a Design of Experiments (DoE) approach. The technique is applied to a conventional laser and plasma welding process as well as to laser-assisted plasma arc welding. In comparison to the individual processes, the laser-assisted plasma arc welding shows a more than doubled overall thermal efficiency, which can be ascribed to a drastic increase in melting efficiency and a moderate increase in energy coupling efficiency.

Introduction

Today, for the fulfilment of a specific welding task, there is a variety of processes available. In order to find out the best-suited process not only the acquisition costs but also the operating costs has to be taken into account. The latter are highly influenced by the overall thermal efficiency η_T, which defines the ratio between the applied and the effectively used energy to melt the base material. The thermal efficiency is commonly split in two separate terms, the energy coupling efficiency η_C and the melting efficiency η_M [1] according to equation (1).

$$\eta_T = \eta_C \cdot \eta_M \tag{1}$$

The energy coupling efficiency in terms of power determines the thermal load of the workpiece and is defined as the ratio between the total applied power P_{tot} and the part of it transferred to the workpiece P_{trans}, see equation (2).

$$\eta_C = \frac{P_{trans}}{P_{tot}} \tag{2}$$

The energy coupling efficiency is the measure of the energy transferred from the heat source to the workpiece. Its value is lowered by primary energy losses of a particular type of heat source to the environment, e.g. reflected radiation in laser material processing or amounts of radiative and convective energy transfer from an arc plasma to the ambient atmosphere in arc welding. In contrast, the value of the melting efficiency η_M is determined by secondary energy losses as a result of heat conduction from the processing zone into the bulk material and of convective and radiative heat transfer from the workpiece to the environment. The melting efficiency in terms of power is defined as ratio of power P_M used to melt the base material to the power P_{trans} transferred to the workpiece, see equation (3).

$$\eta_M = \frac{P_M}{P_{trans}} \tag{3}$$

In the case of laser welding, the relevant efficiency values not only depend on primary process parameters such as wavelength [2], intensity [3], feed rate [4] and material [5]. They are also influenced by the environmental conditions like the applied shielding gas [6], the surface condition and the temperature of the

probe [7]. In consequence, values for process efficiencies differ widely in literature and are seldom reliable approximations of real processes with a particular set of parameters and with consideration of the specific boundary conditions.

Various methods for estimating efficiency values of welding processes were already proposed. Niles and Jackson [4] used an analytical model based on the heat source equation of Rosenthal. The model was calibrated using temperature curves recorded by thermocouples. The authors aimed at estimating the coupling efficiency of a Tungsten Inert Gas (TIG) welding process and derived a correlation between the coupling efficiency and the welding current as well as the feed rate. Kim et al. [8] applied this method to a laser welding process and found a correlation between the coupling efficiency and the feed rate. This method was improved by Cantin and Francis [9] by adding eight thermocouples and performing the experiments inside an isolated box to reduce the systematic error. They found a relationship between the type of inert gas and the coupling efficiency. Gonçalves et al. [10] applied the same method using four thermocouples to determine the coupling efficiency of a TIG process. As has been pointed out, the method can be used to estimate the energy coupling efficiency of laser as well as electrical arc processes. Thus, this allows also the application to a hybrid process. However, the method accompanies a large measuring error by not taking into account the heat distribution inside the probe and the exact location of the measuring points. In order to achieve high accurate estimations, the precise location of the temperature measurement needs to be considered [11].

Another methodology for measuring the heat input is the calorimetry. Colling et al. [12] used a water cooled probe and determined the coupled energy of a TIG welding process through measuring the temperature raise of the cooling water. They also found a correlation between the energy coupling efficiency and the feed rate. Miyamoto et al. [13] conducted laser welding experiments in an argon atmosphere. The probe was subsequently brought to a water calorimeter and the transferred heat to the workpiece was calculated as a function of the mass loss of the water by evaporation. For a laser welding process they derived a dependency of the coupling efficiency on the feed rate. Evans et al. [14] applied this method to a plasma arc welding process and found a correlation of the coupling efficiency and the welding current. According to Pepe et al. [15], the conduction of the experiments outside the calorimeter and the transfer of the probe entails a measuring error of up to five percent. Therefore, Fuerschbach [16] conducted laser beam welding experiments inside a Seebeck-envelop calorimeter, which should reduce the error to two percent. He found a nonlinear correlation between the coupling efficiency and the intensity of the laser. Further studies did not find any evidence for a link between the coupling efficiency and the pulse width as well as the intensity of a pulsed laser beam welding process [17]. Hu and den Ouden [18] used a Seebeck-envelope calorimeter to compare the coupling and melting efficiency of a conventional laser and arc welding process to the combined laser arc hybrid welding. For all three processes they found a coupling efficiency on the same level while the melting efficiency was doubled in the hybrid process. The advantage of this method is the direct measurement of the heat input and the applicability to conventional and hybrid processes. However, the practical application is limited by the long measuring time, which can be up to 11 hours for one run [19]. Furthermore, the measuring error can exceed the reported two percent by coupled energy in the calorimeter walls through scattering. Another source of error is the heat loss through the calorimeter walls because of the long measuring time.

Gonzalez et al. [11] combined the measurement techniques with thermocouples and a calorimeter. The energy loss through convection was measured using a water calorimeter under a cooled copper anode. The heat input to the anode was determined using nine thermocouples and an inverse simulation model. The results of the experiments showed the coupling efficiency of a TIG welding arc. Besides the possibly high accuracy of the measurement, the method is disadvantageous due to the limitation to the material copper. Further, a laser welding process is difficult to realize and determinations under real process conditions are impossible.

In summary, all methods exhibit a large measuring error or the ability to examine both, laser and electrical arc processes, is limited. In this article a new method for determining the coupling and melting efficiency under process conditions is suggested. It can be applied to every kind of heat treatment including laser, electrical arc and hybrid welding and its measuring error is thought to be minimized. The next chapter presents the procedure of the method followed by an examination of the factors that possibly influence the accuracy. The last chapter shows experiments to test and evaluate the method.

Description of the method

The technique to estimate the energy coupling and melting efficiency consists of three parts:

1. The temperature of the probe is experimentally recorded at particular locations outside the processing zone, (i) for the time of the heat source – material interaction during the welding process, and (ii) for the subsequent 300 seconds during the cooling down regime.

2. The measured temperature time curves are brought into agreement with calculated temperature profiles of a corresponding simulation model. Agreement is achieved if the used coupling efficiency value matches the real one. As a result, the coupling efficiency is known for a particular set of process parameters and material properties.

3. The overall thermal efficiency is calculated as a function of the size of the fusion zone. Finally, the melting efficiency is derived according to Equation (1) as ratio of the overall thermal efficiency to the coupling efficiency.

Test execution

A schematic drawing of the experimental setup is shown in Figure 1. The probe is mounted on a thermally isolated clamping device and is moved under the heat source. Four measuring areas *A1-A4* are defined on the probe and coated with graphite. This ensures a homogenous surface condition with defined emission coefficient. The measuring areas with a size of 10x10 mm^2 are located apart the heat source – material interaction zone. Thus, the measuring range remains small and the temperatures can be precisely measured by use of thermography as contactless measuring method. The thermographic camera is located perpendicular over the workpiece to record the temperature distribution within the time of the experiment and the subsequent 300 seconds. The temperature of the measuring areas is averaged to receive the time-temperature curves for the heating and cooling regime of the probe.

Two factors impact the measurement accuracy in this step. First, the measuring error of the camera influences the total accuracy directly. The applied thermographic system has a temperature resolution of 0,025 K with an accuracy range of +/- 1 %. It is expected that for the estimation of efficiency values the temperatures need to be measured with an accuracy of a tenth Kelvin. Therefore, the measuring error of the thermography system is seen to be negligible. Second, the variation of the emission coefficient influences the accuracy of the method. In preliminary tests the emission coefficient of the graphite coated measuring areas in combination with the thermographic camera recording in the wavelength range of λ= 7,5-11 µm was estimated. Four temperature levels in the range of 20 until 100 °C were considered. The determined emissivity value amounted to 0,77 with an variance of +/- 1,25 %. This is in good agreement with the calculated value of 0,83 for the spectral emissivity at 10 µm using data from Nemanich et al. [20]. The influence of the variance of the emissivity on the temperature measurement was then examined and found to be in the range of 0,7 %. Therefore the total measuring error of the first step is better than 1%.

Computational Model

The applied numerical model solves the heat conduction equation by Fourier using a Finite-Difference Method (FDM). In the considered case of metallic sheets with small thickness (1 mm), the

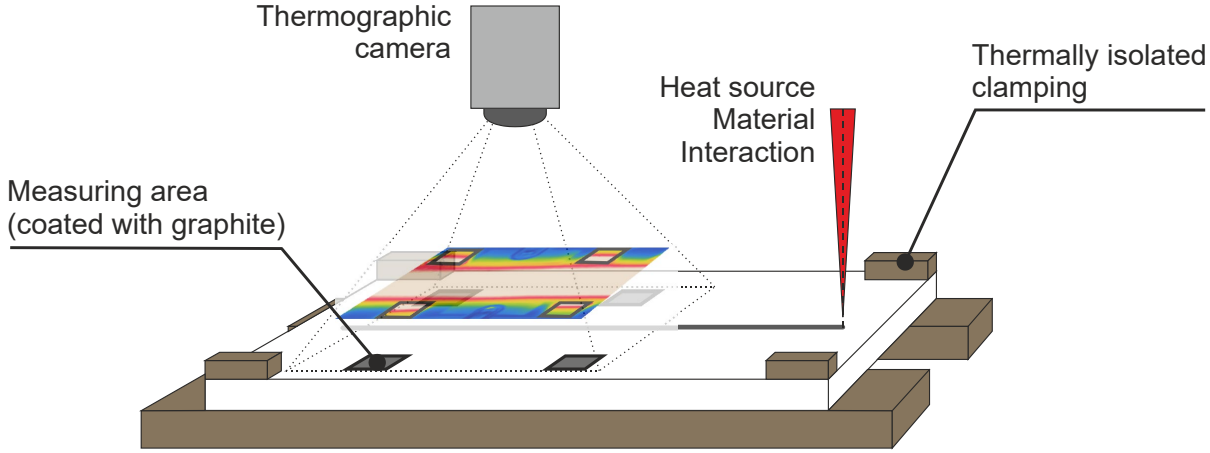

Figure 1 Schematically drawing of the experimental arrangement to estimate the temperature-time curve of a welding process

corresponding value of the Biot number Bi

$$Bi = \frac{\alpha_{tot} * l_{ch}}{\lambda_{th}} \equiv \frac{t_{Sh}/\lambda_{th}}{1/\alpha_{tot}} = \frac{R_\lambda}{R_\alpha} \ll 1 \qquad (4)$$

as the ratio of thermal resistance R_λ to heat transfer resistance R_α with the overall heat transfer coefficient α_{tot}, the sheet thickness t_{Sh} as characteristic length l_{ch} and the thermal conductivity λ_{th} becomes very small and justifies a 2D approach by neglecting temperature gradients over the thickness of the sheet. In that case, the energy input from the laser beam and the arc is described by two independent volumetric source terms $q_{V,L}$ and $q_{V,Arc}$ according to

$$q_{V,L} = \frac{\eta_{C,L} \cdot i_L(r)}{t_{Sh}} = \frac{\eta_{C,L} \cdot 2 \cdot P_L}{t_{Sh} \cdot \pi \cdot r_{0,L}^2} \cdot \exp\left(\frac{-2 \cdot r^2}{r_{0,L}^2}\right) \qquad (5)$$

$$q_{V,Arc} = \frac{\eta_{C,Arc} \cdot i_{Arc}}{t_{Sh}} = \frac{\eta_{C,Arc} \cdot 2 \cdot U_{Arc} \cdot I_{Arc}}{t_{Sh} \cdot \pi \cdot r_{0,Arc}^2} \cdot \exp\left(-\frac{2 \cdot r^2}{r_{0,Arc}^2}\right) \qquad (6)$$

It is obvious that both heat sources are approximated by a normal intensity distribution in radial direction with the effective radii $r_{0,L}$ and $r_{0,Arc}$ of the laser beam and the arc root. Furthermore, i_L and i_{Arc} denote the intensities of the beam and the arc, $\eta_{C,L}$ and $\eta_{C,Arc}$ are the corresponding coupling efficiencies, P_L is the laser power, U_{Arc} the arc voltage and I_{Arc} the arc current.

In addition to the introduced source terms, a loss term $q_{V,Loss}$ considers convective and radiative losses to the environment. Based on the cooling down approach by Newton, the loss term is expressed by

$$q_{V,Loss} = \frac{q_{A,Conv} + q_{A,Rad}}{t_{Sh}} = \frac{(\alpha_{Conv} + \alpha_{Rad}) \cdot (\vartheta(r) - \vartheta_\infty)}{t_{Sh}} \qquad (7)$$

with the convective and radiative heat transfer rates $q_{A,Conv}$ and $q_{A,Rad}$, the corresponding heat transfer coefficients α_{Conv} and α_{Rad} and the ambient temperature ϑ_∞. The radiative heat transfer coefficient follows from the Stefan-Boltzmann law to

$$\alpha_{Rad} = \varepsilon_{eff} \cdot \sigma \cdot \frac{T(r)^4 - T_\infty^4}{\vartheta(r) - \vartheta_\infty} \qquad (8)$$

whereas ε_{eff} denotes the emission coefficient, σ the Stefan-Boltzmann constant and T the absolute value of temperature.

As a first step, the steady-state temperature distribution $\vartheta(x,y)$ at the end position of the heat source (moved at constant speed along a straight path as shown in Figure 1) is computed by the numerical solution of the following governing equation

$$0 = \frac{1}{\rho \cdot c_p} \cdot \left[\frac{\partial}{\partial x}\left(\lambda_{th}\frac{\partial \vartheta}{\partial x}\right) + \frac{\partial}{\partial y}\left(\lambda_{th}\frac{\partial \vartheta}{\partial y}\right)\right] - \frac{\partial (v_x \vartheta)}{\partial x} + \frac{q_{V,Tot}}{\rho \cdot c_p} \qquad (9)$$

as a function of the Cartesian coordinates x and y. The motion of the heat source is considered as convective material flow with the welding speed v_x. Material properties are the density ρ, the specific heat capacity c_P as well as the thermal conductivity λ_{th}. The source term summarizes the input by the applied heat sources as well as the convective and radiative losses according to

$$q_{V,Tot} = q_{V,L} + q_{V,Arc} - q_{V,Loss} \qquad (10)$$

Adiabatic conditions are assumed for the lateral and outflow boundaries whereas a constant temperature ϑ_∞

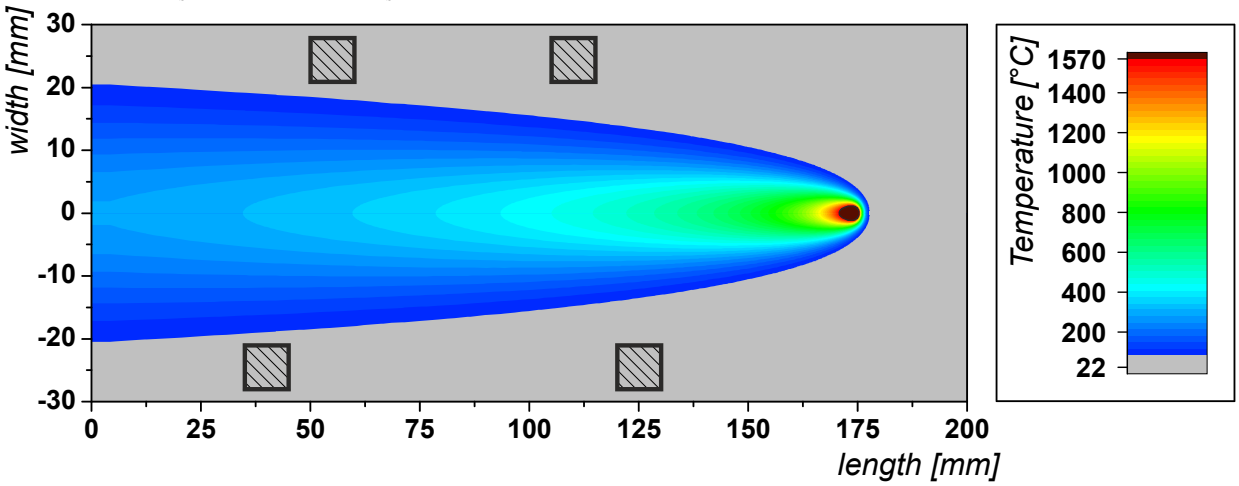

Figure 2 Steady state temperature Distribution of the LaPAW process

is given at the inflow boundary. A calculated steady-state temperature field is exemplarily shown in Figure 2 for a given parameter constellation. This temperature distribution is the initial solution for a second stage in which the temperature distribution is computed as a function of time t on the base of the time-dependent heat conduction equation

$$\frac{\partial \vartheta}{\partial t} = \frac{1}{\rho \cdot c_p} \cdot \left[\frac{\partial}{\partial x}\left(\lambda_{th} \frac{\partial \vartheta}{\partial x} \right) + \frac{\partial}{\partial y}\left(\lambda_{th} \frac{\partial \vartheta}{\partial y} \right) \right] - \frac{q_{V,Loss}}{\rho \cdot c_p} \quad (11)$$

Calculated temperature profiles of the maximal and minimal probe temperatures ϑ_{Max} and ϑ_{Min} as well as the average value ϑ_{Ave} of the probe and the local value averaged over the area of the measuring window A1 are shown in Figure 3.

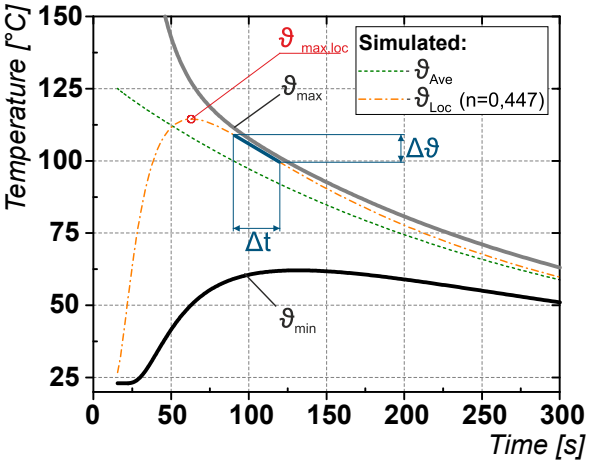

Figure 3 Computed Temperature Curve of the LaPAW process

Determination of efficiency values

The overall thermal efficiency η_T of a welding process can be calculated using equation (12).

$$\eta_T = \frac{P_M}{P_{trans}} = \frac{v_x \cdot A_S \cdot \rho \cdot (c_p \cdot (\vartheta_s - \vartheta_\infty) + h_s)}{U_{Arc} \cdot I_{Arc} + P_L} \quad (12)$$

where v_S is the feed rate, A_S the weld seam area, ρ the density of the probe, c_p the specific heat capacity, ϑ_S and ϑ_∞ the melting point and the ambient temperature, h_s the enthalpy of fusion, U_{Arc} and I_{Arc} the welding voltage and current and P_L the laser power. This formula is applicable for both, conventional laser or electrical arc welding as well as hybrid laser arc welding. With the overall thermal efficiency and equation (1) the melting efficiency can then be determined.

Evaluation of the Computational model

The purpose of the computational model in combination with the thermographic measurements is the determination of the coupling efficiency. It is proposed that the real values can be directly derived from the model if the calculated cooling curve matches the measured one. As shown in Figure 3, the cooling down profiles can be evaluated in a simplified approach by two characteristic quantities, named the temperature maximum $\vartheta_{max,loc}$ and the cooling rate between 90 and 120 s in the corresponding measuring areas. Besides the main process parameters that have a crucial impact on these quantities such as welding speed, arc current and voltage as well as laser power, there are some other uncertain parameters that have to be evaluated with respect to their influence on the cooling curve. For that purpose a sensitivity analysis of the model parameters was performed based on a two level factorial Design-of-Experiments (DoE) approach. Considered factors and corresponding levels are summarized in Table 1.

Table 1 Input factors and assessment parameters for ANOVA

Factor	Level
A. Coupling Efficiency Laser	0,45 | 0,65
B. Coupling Efficiency Plasma Arc	0,45 | 0,65
C. Arc root radius	1,2 | 2,4 mm
D. Heat transfer coefficient	14 | 28 W m^{-2} K^{-1}
E. Emission Coefficient	0,6 | 1,0
F. Ambient Temperature	18 | 24 °C
Assessment parameter	Maximum Temperature Cooling rate 90-120 s

The results of the analysis for both responses - the temperature maximum and the cooling rate - can be found in Figure 4 and Figure 5, illustrated as Half-Normal Plot [21]. Besides the efficiencies as primary parameters also the ambient temperature, the heat transfer coefficient and the emissivity are found to be vital factors. However, the ambient temperature can be measured and its influence on the results of the analysis is minimized in such a way. The emissivity of the measuring areas can be also considered to be known because of the particular preparation with a graphite coating and the preliminary adjustment by own experiments. Finally, the heat transfer coefficient is independent on welding conditions and can also be

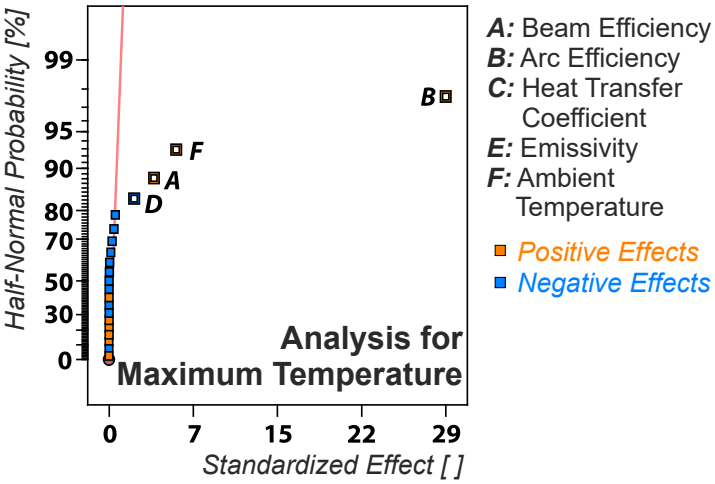

Figure 4 Half-Normal plot for the analysis of the maximum temperature

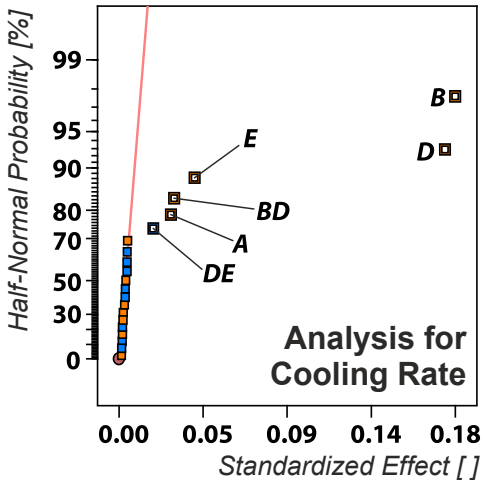

Figure 5 Half-Normal plot for the analysis of the cooling rate between 90-120 s after the process

determined in preliminary experiments. The found value can then be kept constant for a particular test series. An important outcome of the analysis is the finding that the unknown arc root radius does not have any influence on either the maximum temperature nor the cooling rate. The approach of measuring the temperature profiles apart the process zone compensates the variation of arc intensity through heat conduction and the uncertainty regarding this factor can therefore be neglected. In summary, the measured temperature profiles should be perfectly fitted by the correct input of the energy coupling efficiency, i.e. the coupling efficiency of the plasma arc, the laser beam or the combined process. Thus, the model is suited to estimate these values in an inverse computation.

In an additional study, the estimation of the heat input for a steady state approach was compared to a transient calculation. The transient computation was found to be more accurate while being more time consuming. Since the difference between the two approaches was negligible under the condition of a long weld path with respect to the sheet thickness, the steady state approach was used as the initial state for the subsequent transient computation of the temperature fields during the cooling down regime.

Experiments

To test and evaluate the described method, the efficiency values of three different processes (laser, plasma arc and laser assisted plasma arc (LaPAW) welding) are determined. Bead-on-plate welds with a length of 150 mm are conducted on X5CrNi1810 (AISI 304) stainless steel plates with the dimensions of 200x60x1 mm. For the laser process a single mode fiber laser with a maximum power of 600 W is used. The spot diameter amounts to $\omega_0 = 200$ µm and the laser power is fixed at $P_L = 200$ W.

The welding current is $I_{Arc} = 50$ A in the Direct Current Electrode Negative (DCEN) mode for the conventional plasma arc welding process. Argon with a purity of 99,99% is used as both, shielding and plasma gas. The flow rates amount to $Q_{SG} = 10$ l/min for shielding and $Q_{PG} = 0{,}6$ l/min for plasma gas, respectively. The working distance between the plasma nozzle with a diameter of $d_N = 1{,}8$ mm and the workpiece is $z_{WD} = 3$ mm.

The LaPAW process is conducted in a coaxial arrangement, in which the laser beam passes through a hollow cathode. To ensure the comparability of the experiments, the parameters of the individual processes are also used for the LaPAW process ($P_L = 200$ W; $\omega_0 = 200$ µm; $I_{Arc} = 50$ A; $Q_{SG} = 10$ l/min; $Q_{PG} = 0{,}6$ l/min; $d_N = 1{,}8$ mm; $z_{WD} = 3$ mm). The setup was explained in detail by Mahrle et al. [22].

Since there is a correlation between the feed rate and the energy coupling efficiency for an electrical arc welding process [4,12], as well as for laser beam welding [8,13], the feed rate is kept constant for all experiments ($v_f = 0{,}8$ m/min). This enables the comparison of the individual and hybrid process in terms of the determined efficiency values.

Results

In Figure 6 the weld cross section of the three different processes are shown. The seam of the plasma arc process (Figure 6, left) exhibits the typical shape of a heat conduction mode weld. It is shallow and wide with a small aspect ratio and a molten area of 0,7 mm².

This is also applicable to the laser beam welding seam shown in the middle. The low laser power and the comparatively large spot diameter leads to a low power density and to a very small molten area, accordingly (0,06 mm²). The cross section of the LaPAW process exhibits a more than doubled molten area (1,74 mm²) as the sum of plasma and laser weld seam sizes. The heat conduction mode transitions into a deep welding mode in this case and leads to a full root penetration. This phenomenon was described earlier by Steen [23], Fuerschbach [24], Mahrle et al. [22] and others, however, the reason for this effect is still an outstanding issue. The determination of the energy coupling and melting efficiency aims at the clarification of this effect.

Using equation (12) and the molten area from Figure 6, the overall thermal efficiency can be calculated. The values are presented in the lower part of Figure 6. The thermal efficiency of the LaPAW process increases by 115 % in comparison to the individual processes. The additional molten volume doesn't occur because of the higher power in LaPAW but rather because of some still unknown effects that improve the thermal efficiency.

For the determination of the energy coupling efficiency the measured temperature time curves are used to calibrate the calculation model. The curves are shown in Figure 7. It can be seen, that the maximum temperature is perfectly fitted through the calculation model. During laser beam welding the heat input in the base material is small. The process is in the heat conduction mode, wherefore no keyhole is present and the coupling efficiency of the process (η_C = 29,5 %) approximately corresponds to the absorptivity (A= 32,4 %; [25]) of the material. There is also a good match of the experimental and calculated cooling rates in the case of laser welding (see Figure 7 at the bottom).

The maximum temperature of the plasma welding process is much higher and amounts to around 100 °C in the measuring areas. The derived coupling efficiency from these curves evaluates to 37,5 %. This is less than the values documented in literature. DuPont and Marder [26] reported an energy coupling efficiency of 49 %, Evans et al. [14] a range of 49-60 %. A possible reason for this spread can be the comparatively low arc current in the present experiments, and/or it is a consequence of the particular torch design with a hollow cathode. In the case of LaPAW, the energy coupling efficiency is moderately increased by 25 %. This contradicts the results of the experiments by Hu and den Ouden [18], who did not find any increase of coupling efficiency at all. According to Mahrle et al. [27] the improved coupling efficiency can be explained by thermal surface effects. The laser beam strikes the already heated workpiece. Since the absorption of 304 stainless

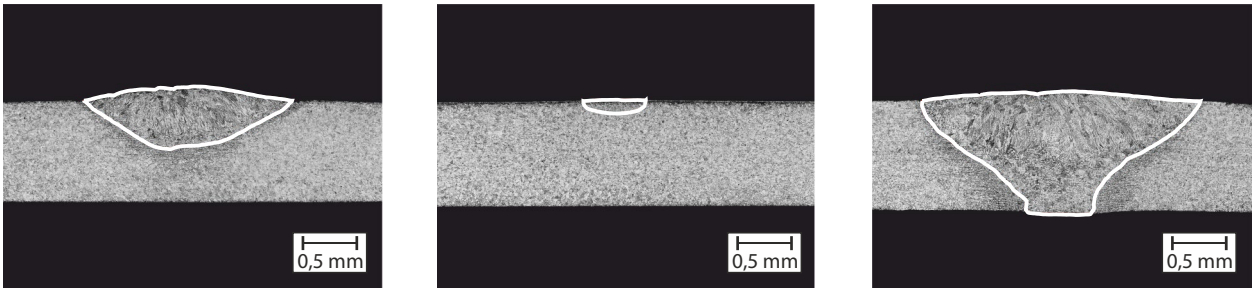

	Plasma	Laser		LaPAW
Thermal Efficiency	0,083	0,034	+115%	0,159
Coupling Efficiency	0,375	0,295	+23,5%	0,447
Melting Efficiency	0,221	0,115	+74,5%	0,356

Figure 6 Weld seam cross section and efficiency values of the Plasma arc (left), laser beam (middle) and LaPAW process (right)

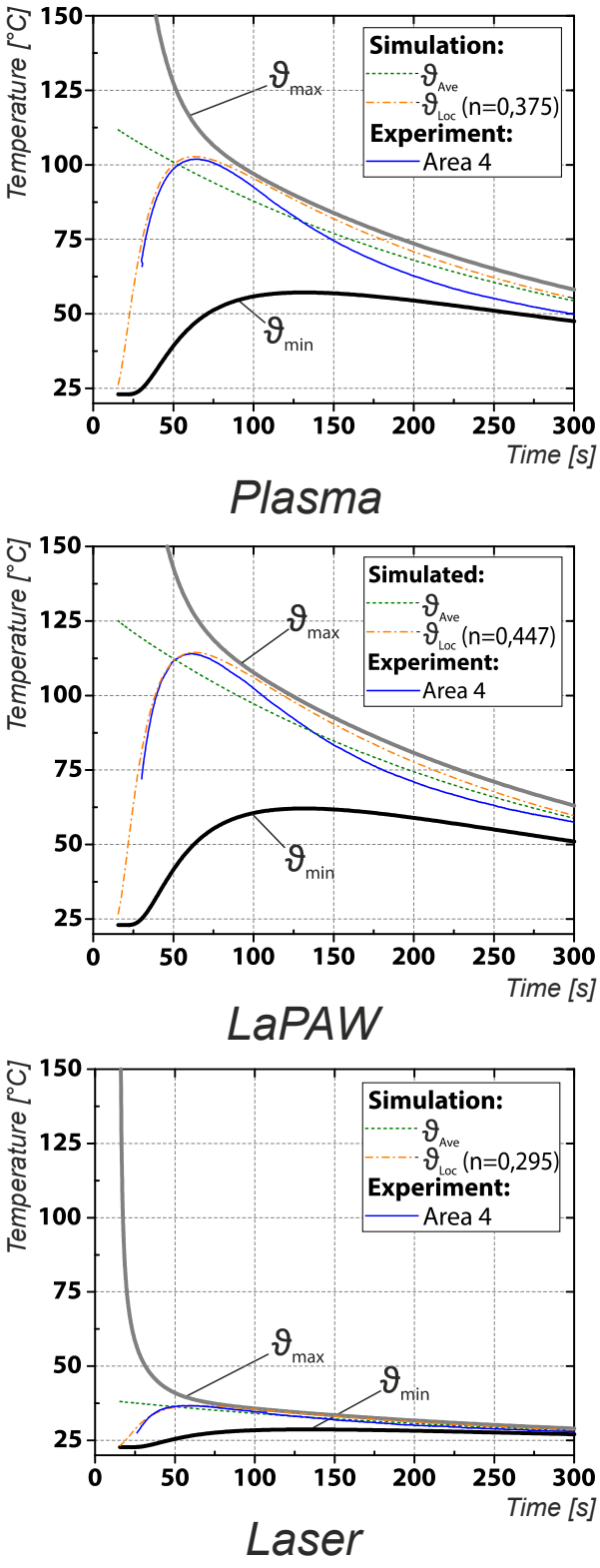

Figure 7 Calculated temperature curves compared to the experiment for a plasma arc (top), LaPAW (middle) and laser beam welding process (bottom).

steel increases with temperature up to 60 % at melting temperature [28], more energy couples into the probe. On the other hand, the hot spot of the laser has possibly an effect on the arc root size.

In Figure 7 at the top and in the middle, it can be seen that the calculation model slightly underestimates the cooling regime of the experiment. A possible explanation for the divergence between the curves can be the 2D calculation model. Although the sheet thickness is small, a 3D model could be needed to capture the experimental tendencies and eliminate surface effects, that are not considered in the 2D model. However, because the difference is 3,5 K in the maximum case, the influence on the calculated coupling efficiency is seen to be low.

The melting efficiency of the LaPAW process is drastically increased by 75 % (see Figure 6). This indicates changes of the thermal characteristic within the processing zone. The coupled energy is more efficiently used to melt the material and heat conduction losses are much probably reduced. This supports the thesis, that secondary effects are responsible for the drastic increase in melt volume occurring during hybrid welding [27]. Also this result is an indication against the theory of an direct interaction of the two involved heat sources as a reason for the synergetic effects [29–31]. If there would be a direct interaction, the coupling efficiency should increase while the melting efficiency, which is mainly influenced through secondary effects of the weld pool, should remain constant. However, a more extensive study has to be conducted to verify these tendencies.

Conclusion

A new method for determining thermal, energy coupling and melting efficiency of welding processes is presented. An inverse calculation is used to fit a 2D heat flow model to experimentally derived temperature-time curves. The calculation model was evaluated in an analysis to identify factors affecting the measuring accuracy. It could be shown, that the curves of the calculation model and the experiment only converge to each other under the premise of the exact input of the energy coupling efficiency value. Therefore, the model is suitable to estimate the energy coupling efficiency value. The overall systematic error of the method consists of the measuring error of the temperature measurement (appx. 0,7 %) and the estimation error of the calculation model (appx. 1,3 %). In total the measuring error of the method is in the range of 2 %.

For testing and evaluating the method, experiments on AISI 304 were conducted. The efficiency values of a

laser beam, a plasma arc and a laser assisted plasma arc welding process were determined and compared. For the laser welding process a perfect fit of the curves was reached. Maximum temperature as well as the cooling regime is perfectly described through the model. However, there is a lack between the cooling regime of the plasma and LaPAW experiment and the theoretically derived curves. This was ascribed to the 2D calculation approach of the heat distribution and heat conduction. The influence on the estimated efficiency values is seen to be small. This fact will be a topic of further studies to increase the measuring accuracy.

In the case of LaPAW, the analysis shows a moderate increase in energy coupling and a drastic increase in melting efficiency compared to the conventional processes. This indicates that the deep welding phenomenon during LaPAW is based on secondary effects, which might change the melt pool behavior and/or favor a keyhole formation. Extensive studies are planned to verify these hypotheses.

It was shown, that the presented method can be applied to conventional laser and electrical arc processes as well as hybrid welding processes. It is applicable under real process conditions. This enables the direct comparison of competing technologies. Therefore it establishes a useful basis for a mathematical consideration of the process and the thermal loads as a consequence thereof. Further, it is a good instrument to fathom basic effects of processes, revealing physical cause-effect relationships and creating new optimization potentials.

Acknowledgment

The authors appreciate the financial support given by the German Research Foundation (DFG) within the project “Experimentelle und theoretische Analyse des Tiefschweißeffektes beim lasergestützten Plasma-schweißen”, Contract No. BE 1875/34-1 and FU307/10-1.

References

[1] Swift-Hook, D.T.& Gick, A.E.F. (1973) Penetration Welding with Lasers, Welding Journal 52, 492–499.

[2] Dausinger, F.& Shen, J. (1993) Energy Coupling Efficiency in Laser Surface Treatment, ISIJ International 33, 925–933.

[3] Fabbro, R., Slimani, S.& Coste, F., et al. (2005) Study of keyhole behaviour for full penetration Nd–Yag CW laser welding, Journal of Physics D: Applied Physics 38, 1881–1887.

[4] Niles, R.W.& Jackson, C.E. (1975) Weld Thermal Efficiency of the GTAW Process, Welding Journal 54, 25–32.

[5] Fuerschbach, P.W.& Knorovsky, G.A. (1991) A Study of Melting Efficiency in Plasma Arc and Gas Tungsten Arc Welding, Welding Journal 70, 287–297.

[6] Åström, H., Stenbacka, N.& Hurtig, K. (2013) Arc Efficiency for Gas Tungsten Arc Welding DCEN-GTAW, Research Report, University West, Trollhättan, Sweden.

[7] Konov, V.I.& Tokarev, V.N. (1983) Temperature Dependence of the Absorptivity of Aluminum Targets at the 10.6 μm Wavelength, Soviet Journal of Quantum Electronics 13, 177–180.

[8] Kim, T.H., Albright, C.E.& Chiang, S. (1990) The Energy Transfer Efficiency in Laser Welding Process, Journal of Laser Applications 2, 23–28.

[9] Cantin, G.M.D.& Francis, J.A. (2005) Arc power and efficiency in gas tungsten arc welding of aluminium, Science and Technology of Welding and Joining 10, 200–210.

[10] Gonçalves, C.V., Vilarinho, L.O.& Scotti, A., et al. (2006) Estimation of heat source and thermal efficiency in GTAW process by using inverse techniques, Journal of Materials Processing Technology 172, 42–51.

[11] Gonzalez, J.J., Freton, P.& Masquère, M. (2007) Experimental Quantification in Thermal Plasma Medium of the Heat Flux Transferred to an Anode Material, Journal of Physics D: Applied Physics 40, 5602–5611.

[12] Collings, N., Wong, K.Y.& Guile, A.E. (1979) Efficiency of tungsten-inert-gas arcs in very-high-speed welding, Proceedings of the Institution of Electrical Engineers 126, 276–280.

[13] Miyamoto, I., Maruo, H.& Arata, Y. (1986) Beam Absorption Mechanism in Laser Welding, Proceedings of SPIE - The International Society for Optical Engineering 668, 11–18.

[14] Evans, D.L., Huang, D.& Mcclure, J.C., et al. (1998) Arc Efficiency of Plasma Arc Welding, Welding Journal 77, 53–58.

[15] Pépe, N., Egerland, S.& Colegrove, P.A., et al. (2011) Measuring the Process Efficiency of Controlled Gas Metal Arc Welding Processes, Science and Technology of Welding and Joining 16, 412–417.

[16] Fuerschbach, P.W. (1996) Measurement and Prediction of Energy Transfer Efficiency in Laser Beam Welding, Welding Journal 75, 24–34.

[17] Fuerschbach, P.W.& Eisler, G.R. (2002) Effect of Laser Spot Weld Energy and Duration on Melting and Absorption, Science and Technology of Welding and Joining 7, 241–246.

[18] Hu, B.& den Ouden, G. (2005) Synergetic effects of hybrid laser/arc welding, Science and Technology of Welding and Joining 10, 427–431.
[19] Hu, B. (2002) Nd/YAG Laser-Assisted Arc Welding, Ph.D. Thesis, Delft University of Technology, Delft.
[20] Nemanich, R.J., Lucovsky, G.& Solin, S.A. (1977) Infrared Active Optical Vibrations of Graphite, Solid State Communications 23, 117–120.
[21] Anderson, M.J. & Whitcomb, P.J. (2007) DOE Simplified: Practical Tools for Effective Experimentation, 2nd edn., Productivity Press, 241 pp.
[22] Mahrle, A., Rose, S.& Schnick, M., et al. (2013) Laser-assisted plasma arc welding of stainless steel, Journal of Laser Applications 25, 32006-1 - 32006-8.
[23] Steen, W.M. (1980) Arc augmented laser processing of materials, Journal of Applied Physics 51, 5636–5641.
[24] Fuerschbach, P.W. (2000) Laser Assisted Plasma Arc Welding, in *ICALEO '99*, 102–109.
[25] Bergström, D., Powell, J.& Kaplan, A.F.H. (2007) The Absorptance of Steels to Nd:YLF and Nd:YAG Laser Light at Room Temperature, Applied Surface Science 253, 5017–5028.
[26] DuPont, J.N.& Marder, A.R. (1995) Thermal Efficiency of Arc Welding Processes, Welding Journal 74, 406–416.
[27] Mahrle, A., Rose, S.& Lohse, M., et al. (2014) Interaction mechanisms in hybrid laser arc welding, in *ICALEO 2014,* San Diego, CA, USA, 1202.
[28] Kwon, H., Baek, W.-K.& Kim, M.-S., et al. (2012) Temperature-dependent absorptance of painted aluminum, stainless steel 304, and titanium for 1.07 μm and 10.6 μm laser beams, Optics and Lasers in Engineering 50, 114–121.
[29] Kozakov, R., Emde, B.& Pipa, A.V., et al. (2015) Change of electrical conductivity of Ar welding arc under resonant absorption of laser radiation, Journal of Physics D: Applied Physics 48, 1–11.
[30] Möller, F.& Thomy, C. (2013) Interaction Effects between Laser Beam and Plasma Arc in Hybrid Welding of Aluminum, Physics Procedia 41, 81–89.
[31] Ribic, B., Palmer, T.A.& DebRoy, T. (2009) Problems and issues in laser-arc hybrid welding, International Materials Reviews 54, 223–244.